

# Out of equilibrium dynamics of quench-induced spontaneous symmetry breaking and topological defect formation

Nuno D. Antunes

*School of Mathematical and Physical Sciences, University of Sussex, Brighton BN1 9QH, United Kingdom*

Luís M. A. Bettencourt

*The Blackett Laboratory, Imperial College, London SW7 2BZ, United Kingdom*

(Received 17 May 1996)

We study the full out-of-thermal-equilibrium dynamics of a relativistic classical scalar field through spontaneous symmetry breaking. In these circumstances we determine the evolution of the ensemble averages of the correlation length and topological defect densities. This clarifies many aspects of the nonperturbative dynamics of fields in symmetry-breaking phase transitions and allows us to comment on a quantitative basis on the canonical pictures for topological defect formation and evolution. We also compare these results to those obtained from the field evolution in the Hartree approximation or using the linearized theory. By doing so we conclude about the regimes of validity of these approximations. [S0556-2821(96)05624-X]

PACS number(s): 11.15.Tk, 11.27.+d, 11.30.Qc

## I. INTRODUCTION

The formation of topological defects is a general consequence of symmetry-breaking phase transitions in field theories with a topologically nontrivial vacuum manifold, both in the early Universe [1,2], and in a number of materials in the laboratory [3–5].

To date predictions of the number and distributions of defects formed in these circumstances has relied on very simplistic heuristic models where some qualitative aspects of the phase transition are invoked, but where all dynamics is sacrificed [6]. These are at the basis of large-scale simulations of defect networks subsequently used to generate the energy density perturbations responsible for the formation of structure in the Universe [7].

Recently, considerable effort has been devoted to the development of more realistic defect formation scenarios based on more sophisticated thermal arguments [8], applicable in the context of a second-order phase transition. These appear consistent with the results of recent experiments in  $^3\text{He}$  and  $^4\text{He}$ . Simultaneously the search for methods to follow the approximate evolution of relativistic field theories in out of equilibrium settings [9–11] has known a considerable improvement, made possible by the utilization of large-scale computing facilities. The first attempts to account for the number of defects formed in this context [12] also have been developed.

In this paper we perform the first complete fully nonlinear dynamical study of a relativistic classical theory out of thermal equilibrium in a symmetry breaking phase transition. We compute the time evolution of many quantities of interest, such as the correlation length and the defect densities as well as their dependence on the choice of initial conditions and on the presence of external dissipation.

We then compare these results to other approaches found recently in the literature. We will show by explicit computation of the time evolution for the zero densities of our field in well-specified and illustrative circumstances, that both the Hartree approximation and the linearized theory have differ-

ent merits in approximating the full classical evolution. By virtue of this comparison we also learn, in a quantitative manner, when they fail and, consequently, about the regimes of their applicability.

The results of this paper raise many extremely interesting new questions concerning the nonperturbative dynamics of relativistic fields away from thermal equilibrium. Our present methods rely heavily on the usage of extensive computational facilities. Rather than openly trying to tackle some of these new issues, the intention of the presentation below will be a more modest one, restricted in its character to that of reporting on the finds of a numerical experiment. A more analytical approach must be sought in order to complete our understanding, though, and it is our intention to expand on our attempts in forthcoming publications. Nevertheless, we believe the present results constitute considerable quantitative progress on the usual canonical qualitative pictures of defect formation and evolution.

This paper is organized as follows. In Sec. II we describe the theoretical background for the field evolution. We discuss the field equations for the full classical evolution in the presence of external dissipation, and our choice of initial conditions, which for consistency we take to follow a classical Boltzmann distribution. We then describe two approximation schemes to the classical evolution, namely, the Hartree approximation and the linearized theory. In the latter case we present the exact analytical evolution and Halperin's formula for the zero densities of the scalar field in a Gaussian theory. We finish this section by describing briefly our numerical procedure for the full classical evolution and the computation of approximate statistical ensemble-averaged quantities.

In Sec. III we present our results. We show the fully non-equilibrium evolution of the scalar field correlation length as well as its zero and defect densities. We show explicitly that the latter can be counted at a given sensible field coarse-graining scale, independently of the necessary ultraviolet cutoff of our implementation. We also discuss the dependence of these results on our choice of initial conditions. We

then proceed to compare these zero densities to those obtained from the Hartree approximation and the linearized theory, and to draw conclusions about the regimes of their applicability. Finally, we present the evolution of the defect densities per correlation volume and seek to relate our results to the qualitative canonical arguments for defect formation and long-time evolution: the Kibble mechanism and scaling conjectures.

In Sec. IV we summarize our most important results, present our conclusions, and point to questions, raised by the present work, which we intend to study in the near future.

## II. THEORETICAL BACKGROUND

In what follows we will be concerned solely with the evolution of a *classical* relativistic field theory. The role of quantum fluctuations on the evolution of our field is, therefore, simply neglected. This is done in the spirit of statistical relativistic field theories, e.g., [13].

Our neglect of all quantum aspects should, however, constitute an excellent approximation to the complete field dynamics at energies close to the phase transition temperature. This is a nontrivial statement to quantify in general, but that can be made precise by treating the presence of the nonlinear term in the usual perturbative loop expansion. The fundamental difference between the thermal and the quantum loop perturbative series then arises from the fact that the quantum expansion is organized in terms of increasing powers of  $\hbar$  while the thermal one is proportional to powers of the temperature  $T=1/\beta$ , made adimensional by appearing explicitly in ratios with the mass scales in the theory. In the regime in which the temperature to mass ratios are very large compared to  $\hbar$ , quantum fluctuations can be neglected safely relative to their thermal equivalent. Another manifestation of the quantum nature of a field theory is that the energy spectrum becomes discrete and, consequently, the thermal distribution becomes Bose-Einstein instead of its classical Boltzmann form. Both classical and quantum distributions coincide approximately for frequencies  $\omega$  such that  $\hbar\omega/T \ll 1$ , showing again that quantum manifestations should become fundamental in the ultraviolet of the theory and/or at low temperatures, as is well known. Both these regimes are relatively unimportant for the studies presented below and, given our choice of the initial field configurations, may be probed only under extreme conditions in the evolution or measurements performed over the deep ultraviolet sector of the theory. We will not be concerned with these regimes below and that, given the fundamental difficulties inherent to a full quantum approach relative to the opportunities offered by the classical theory, constitutes our best justification for neglecting quantum fluctuations. Although somewhat unsatisfactory, we believe this is in itself justifiable in view of the extremely interesting possibilities it permits, especially in opening a window for probing nonperturbative aspects of the field evolution at the phase transition. In this section we will proceed to describe the details of our full classical evolution as well as the basis for two approximations, the Hartree self-consistent evolution and the linearized theory. We conclude this section by presenting the predictions from the exact results possible in Gaussian theories and discussing our numerical methods.

### A. The classical theory

In what follows we will adopt the simplest collisional model displaying topological defects, i.e., we will be dealing with a classical  $\lambda\phi^4$  scalar field theory in 1+1 dimensions. In one spatial dimension, a Boltzmann distributed classical field is always finite and, therefore, does not require renormalization [13]. This choice of spatial dimensionality also allows us to guarantee, from a technical point of view, that we will be able to evolve numerically a discretized dynamical system with enough resolution on all scales and generate a sufficiently large number of field realizations in order to be able to compute true statistical ensemble-averaged quantities. In one spatial dimension and in equilibrium, the Mermin-Wagner theorem [14] states that there is no long-range order. In this sense there is no phase transition as understood canonically in terms of thermodynamic quantities. In an out-of-equilibrium evolution such as ours, however, spontaneous symmetry breaking certainly occurs, in the sense that the field chooses locally in space to fall towards either of the energetically equivalent minima. In what follows we, therefore, will continue to use the term symmetry breaking phase transition in this sense. In any case, equilibrium in our evolution, as will be clear by the end of this section, can be strictly achieved only at zero temperature, where the Mermin-Wagner theorem ceases to apply. Field theories in higher spatial dimensions will be considered in a forthcoming work [15].

In order to trigger the transition, we set up initially a large number of field configurations out of a canonical statistical ensemble and, at  $t=0$ , destabilize the system by changing instantaneously the sign and magnitude of the mass.

The evolution equations for  $t>0$ , then will be taken to be

$$(\partial_t^2 - \nabla^2)\phi - m^2\phi + \lambda\phi^3 + \eta\dot{\phi} = 0, \quad (2.1)$$

where  $\lambda$  is the scalar self-coupling and  $m$  is the classical mass. The dissipation coefficient  $\eta$  is included as we wish to describe a system in the presence of additional degrees of freedom. This is a necessary condition in order to justify the use of a canonical thermal distribution of fields as our initial conditions. Accordingly, the form of the evolution equations can be obtained exactly if our system, the scalar field, is assumed to be in contact with a much larger one, a thermal bath of oscillators, coupled linearly to  $\phi$ . The result is a Langevin system with a simple Markovian dissipation kernel, characterized only by the constant value of  $\eta$ , and a noise term, where the two are related by the fluctuation-dissipation theorem [16]. At zero bath temperature and in the absence of quantum fluctuations, the system reduces to Eq. (2.1).

It is convenient and physically clarifying to consider the rescaled system by redefining the time and space variables as well as the field amplitudes as in

$$x \rightarrow x/m, \quad t \rightarrow t/m, \quad \phi \rightarrow \sqrt{\lambda/m}\phi, \quad (2.2)$$

to be

$$(\partial_t^2 - \nabla^2)\phi - \phi + \phi^3 + \tilde{\eta}\partial_t\phi = 0, \quad (2.3)$$

where

$$\tilde{\eta} = \eta/m. \quad (2.4)$$

The new dissipation constant  $\tilde{\eta}$  has a clear physical interpretation. It is the ratio of the wavelength  $1/m$ , for the mean scalar field to the diffusion length,  $1/\eta$ , of a free Brownian particle in contact with the thermal bath. Whenever this ratio is small, the diffusion length is large compared to the particle's wavelength and the only collisional effects present involve the interaction of the scalar field with itself. In the converse limit the system is dominated by dissipative effects to the bath and the dynamics obey essentially a diffusion equation where the second derivative in Eq. (2.3) is negligible relative to the first and as a consequence oscillations and self-interactions play a secondary role.

The ratio  $\tilde{\eta}$  is, therefore, our fundamental dynamical parameter. All other information about the system is encoded in the initial field configurations. To specify these we assume that, for  $t < 0$ , the system will be described by a free-field equation, with possibly a different mass parameter  $M$ ,

$$(\partial_t^2 - \nabla^2)\phi + M^2\phi = 0, \quad (2.5)$$

in thermal equilibrium at a given temperature  $1/\beta$ . Our goal is to compute ensemble averages of several quantities throughout the evolution. In order to achieve this we generate initially a large number of field configurations out of a Boltzmann distributed statistical ensemble. This is, of course, the classical canonical equilibrium distribution. The probability density functional,  $P[\phi, \Pi]$ , for the field and its canonical conjugate momentum  $\Pi = \partial\phi/\partial t$  will be given by

$$P[\phi, \Pi] \propto e^{-\beta\mathcal{H}[\phi, \Pi]}, \quad (2.6)$$

where  $\mathcal{H}$  is the free-field Hamiltonian

$$\mathcal{H}[\phi, \Pi] = \frac{1}{2} \int_0^L dx \Pi^2(x) + \left( \frac{\partial\phi}{\partial x}(x) \right)^2 + M^2\phi^2(x), \quad (2.7)$$

where  $L$  is the one-dimensional volume of our system, which will be taken to be much larger than the mean correlation length of the initial field configuration  $\xi = 1/m$ .

Since this is a Gaussian distribution, we need specify only the mean value and variance for the field and its conjugate momentum in order to characterize it. We do this most simply in Fourier space, where we have

$$\langle \phi_k(0) \rangle = 0, \quad \langle \phi_k(0) \phi_{-k}(0) \rangle = \frac{1}{\beta L \omega_k^2} \quad (2.8)$$

and

$$\langle \Pi_k(0) \rangle = 0, \quad \langle \Pi_k(0) \Pi_{-k}(0) \rangle = \frac{1}{\beta L} \quad (2.9)$$

with the dispersion relation

$$\omega_k = \sqrt{k^2 + M^2}, \quad |k| = \frac{2\pi n}{L}, \quad n = 0, 1, \dots, +\infty. \quad (2.10)$$

The same statistical field configuration could have been obtained by driving a linear (i.e., free of self-interactions)

field to thermal equilibrium in contact with a reservoir at temperature  $1/\beta$ , using a Langevin evolution equation [13].

In order to trigger the symmetry breaking transition, we proceed, at  $t=0$ , to change instantaneously  $M^2$ , in sign and in magnitude, thus forcing the system to leave thermal equilibrium and to evolve in a nonlinear way, according to Eq. (2.1). This is the simplest way of destabilizing the system and has the advantage of analytical tractability in the simplest cases. Because of this property it has been used extensively in the literature [9,12], where the instantaneous change of  $M^2$  is often referred to as a *quench*. In terms of bulk thermodynamical quantities, it corresponds to a sudden decrease in Pressure, or in the language of finite temperature field theory, a decrease in the theory's effective potential. It is not clear to us, however, if such a triggering mechanism has a natural implementation in the laboratory.

In order to compute average quantities, we then evolve numerically a large number of random field realizations out of the statistical ensemble Eqs. (2.8) and (2.9), using Eq. (2.1) and compute, at given time intervals, their mean values over this set.

Before we proceed to present our results, we will describe briefly two approximate schemes to the evolution described above, the Hartree approximation and the linearized theory. In the next section we will compare the results obtained by these three different approaches.

## B. The Hartree approximation

A widely used approximation scheme to the full approach described in the previous section is the so called Hartree self-consistent approximation [19]. Unlike the naive perturbative expansion, it has the virtue of remaining stable throughout the symmetry breaking transition. It is also fully renormalizable in the case of quantum initial conditions [10,11]. Because of these characteristics, the Hartree approximation has received quite a lot of attention in the recent literature as a means of performing out-of-equilibrium computations in various situations [10,11].

As a drawback it describes a theory where all energy transfers must be made through the mean-field and, as a consequence, in situations when the field evolution involves important energy transfers among modes with  $k \neq 0$ , it behaves poorly. Our objective below will be to make the latter statement more precise.

The Hartree approximation results from making the Lagrangian quadratic, by replacing the quartic term by an expression involving only the average value of the quadratic field. More interestingly, it can be seen to arise as the first order in a systematic perturbative expansion, in the parameter  $1/N$  of an  $O(N)$  symmetric theory, see, e.g., [11].

Once this form for the Lagrangian density is assumed, the corresponding evolution equations are required to be self-consistent, in the sense that the zero separation two-point

<sup>1</sup>It is clear that this is not the mechanism of destabilizing the theory in a cosmological context. Pressure quenches were used to drive liquid <sup>4</sup>He systems through a superfluid phase transition [3], but are thought to be accompanied by other energy loss mechanisms.

function computed at each step of the evolution is the same one present in the effective Lagrangian, for the corresponding time.

In practice this can be achieved by replacing the cubic term in the Euler-Lagrange equation by

$$\phi^3(t,x) = 3\langle\phi^2(t)\rangle\phi(t,x). \quad (2.11)$$

With this substitution the approximate evolution equations now describe a Gaussian field with an effective time-dependent mass. This allows us to compute easily the time-dependent two-point function  $W(x,x',t,t')$ :

$$\begin{aligned} W(x,x',t,t') &= \langle\phi(x,t)\phi(x',t')\rangle \\ &= \sum_{k=-\infty}^{+\infty} G_k(t,t')e^{ik(x-x')}, \end{aligned} \quad (2.12)$$

where we chose to write  $G_k(t,t')$  in terms of the usual positive and negative frequency modes,  $U_k^+(t)$  and  $U_k^-(t)$ , respectively, as

$$G_k(t,t') = U_k^+(t)U_k^-(t') + U_k^-(t)U_k^+(t'). \quad (2.13)$$

These, in turn, obey the field evolution equations

$$\left[ \frac{d^2}{dt^2} + k^2 - m^2 + 3\lambda\langle\phi^2(t)\rangle + \eta\frac{d}{dt} \right] U_k^\pm(t) = 0. \quad (2.14)$$

The initial conditions Eq. (2.8) and (2.9), also can be written in terms of the positive and negative frequency modes  $U_k^+(t)$  and  $U_k^-(t)$ . We obtain

$$U_k^\pm(t=0) = \frac{1}{\omega_k\sqrt{2\beta L}}, \quad \dot{U}_k^\pm(t=0) = \frac{\pm i}{\sqrt{2\beta L}}. \quad (2.15)$$

For the Hartree scheme to be complete, we have to impose a consistency equation, namely, that the mean-field taken in Eq. (2.14) be the same as the result obtained from two-point correlation function calculated from Eq. (2.13). This gives

$$\langle\phi^2(t)\rangle = 2 \sum_{k=-\infty}^{+\infty} U_k^+(t)U_k^-(t). \quad (2.16)$$

Equations (2.14) and (2.16) together with the initial conditions Eq. (2.15) constitute a well-posed initial value problem that can easily be solved numerically, for a discretized set of momenta. Note that once we obtain the time-dependent correlation function, we have at our disposal all the information about the system since the Hartree approximation assumes implicitly a Gaussian distribution of fields.

Equation (2.14) shows that the Hartree approximation is clearly collisionless as it describes the interactions of an infinite set of modes with a mean-field. As a result energy transfer processes among the modes proceed without any exchange of momentum, necessarily through the mean-field. The collisionless character of the Hartree approximation constitutes its greatest weakness and will bring about substantial differences to the behavior observed by evolving the scalar field using Eq. (2.1), as we will illustrate in the next section.

### C. The linear approximation

More severely, one can neglect the interactions altogether simply by removing the cubic term in the evolution from Eq. (2.1). This is necessarily an extremely crude approximation, but has the merit of making it possible to predict, given an initial Gaussian field configuration, all the relevant quantities analytically. It also can be assumed (as it has been done frequently in the literature, see [12]) that for certain parameter ranges the relevant evolution occurs in the period soon after the field leaves equilibrium and starts descending towards the minimum of the new potential. During this stage the potential can, in fact, be approximated by an inverted squared well, but as we will see later the nonlinear aspects of the evolution will in well-defined circumstances be relevant for the mechanism of defect production, altering substantially their numbers.

Since the evolution is linear, the distribution of fields will remain Gaussian for all times and we need to determine only the two-point correlation function in order to have a full description of the system. This can be done analytically, with the positive and negative frequency modes being given by

$$U_k^+(t) = \frac{e^{-\eta/2t}}{\sqrt{2\beta L}} \left[ \frac{1}{\omega_k} \cosh(\Omega_k t) + \frac{i}{\Omega_k} \left( 1 - \frac{i\eta}{2\omega_k} \right) \sinh(\Omega_k t) \right], \quad |k| < k_c, \quad (2.17)$$

$$U_k^+(t) = \frac{e^{-\eta/2t}}{\sqrt{2\beta L}} \left[ \frac{1}{\omega_k} \cos(\Omega_k t) + \frac{i}{\Omega_k} \left( 1 - \frac{i\eta}{2\omega_k} \right) \sin(\Omega_k t) \right], \quad |k| > k_c,$$

with

$$U_k^-(t) = (U_k^+)^*,$$

where  $\Omega_k = \sqrt{|k^2 - m^2 - \eta^2/4|}$  and  $k_c = \sqrt{m^2 + \eta^2/4}$ . Note that, modulo the effect of the external dissipation that damps all modes, the evolution is divided in the usual way between exponential (for  $|k| < k_c$ ) and oscillatory (for  $|k| > k_c$ ).

### D. Analytical results for the Gaussian theory—counting zeros and defects

In the special case of the linearized evolution exact analytical predictions are possible, which constitute an excellent test on our methods. These results are based on a well-known computation, first derived by Halperin [17]. Given the knowledge of the equal time two-point function and its spatial derivatives, it allows us to calculate the average spatial density of zeros  $\langle n_0 \rangle$ , in a Gaussian distribution of fields. In one dimension Halperin's formula becomes

$$\langle n_0(t) \rangle = \frac{1}{\pi} \sqrt{\left| \frac{W''(0,t)}{W(0,t)} \right|}, \quad (2.18)$$

where, by translational invariance,

$$W(x,x',t) = W(|x-x'|,t) \equiv W(r,t). \quad (2.19)$$

One of the simplest applications of this result is for the case of a Boltzmann distribution of free quadratic fields, which corresponds to our initial conditions. We then have that our two-point function is explicitly time independent and takes the form

$$W(x, x') = \frac{1}{\beta L} \sum_{k=-\infty}^{+\infty} \frac{1}{\omega_k^2} e^{ik(x-x')}, \quad (2.20)$$

on a discrete periodic lattice, with  $k$  and  $\omega$  obeying the dispersion relation Eq. (2.10). When substituted in Eq. (2.18) this gives

$$\langle n_0 \rangle = \frac{1}{\pi} \sqrt{\frac{\sum_{k=-\infty}^{\infty} k^2 / \omega_k^2}{\sum_{k=-\infty}^{\infty} 1 / \omega_k^2}}. \quad (2.21)$$

It is clear that  $\langle n_0 \rangle$ , given by Eq. (2.21), diverges. Introducing an upper momentum cutoff  $\Lambda$  we have that this divergence is of the form  $\langle n_0 \rangle \sim \Lambda^{1/2}$ .<sup>2</sup>

Equation (2.18) can be extended easily to both the Hartree and the linear evolutions, since in both cases the field distributions remain Gaussian for all times. This fact allows us to obtain a time-dependent zero density, which can be written explicitly in terms of the propagating modes as

$$\langle n_0(t) \rangle = \frac{1}{\pi} \sqrt{\frac{\sum_{k=-\infty}^{+\infty} k^2 |U_k^+(t)|^2}{\sum_{k=-\infty}^{+\infty} |U_k^+(t)|^2}}. \quad (2.22)$$

As before the result diverges clearly. This can be seen from the explicit analytical result, in the linear case, or numerically for the Hartree approximation. This divergence is a consequence of the existence of too large a number of zeros in arbitrarily small scales, too large in fact for the series in Eq. (2.22) to converge to a finite result. The number of zeros that correspond to defects is, however, clearly independent of the behavior of the field deep in the ultraviolet. In order to measure the correct number of defects present in a given field configuration with zero crossings on all scales, we, therefore, must introduce a coarse-graining scale, which we, naturally, will choose to be of the order [usually slightly larger] than the size of a defect [18]. In one spatial dimension there is an exact domain wall solution with a well-defined width, given by  $1/m$ .

When evolving the full nonlinear theory, we, thus, will have to introduce two relevant scales. An upper momentum cutoff  $\Lambda$  which is related to the number of modes chosen to generate the initial conditions, and a coarse-graining scale, of the order of  $1/m$ , used for calculating the defect density. This density then has to be shown explicitly not dependent on the upper momentum cutoff. Given this cutoff scale, we also will measure the zero density and compare it to the analytical predictions both from the linear and Hartree approximations.

### E. The numerical evolution

In order to perform the nonlinear out-of-equilibrium evolution, we have used a 128-processor parallel computer. We

<sup>2</sup>For spatial dimension  $D=2$ ,  $\langle n_0 \rangle \sim \Lambda^2 / \ln(\Lambda)$ . For  $D \geq 3$ ,  $\langle n_0 \rangle \sim \Lambda^D$ .

took advantage of this architecture to evolve in each processor a different random realization of the initial Boltzmann distributed scalar field. For each one of these, we took the initial ultraviolet cutoff to correspond to a wave number of about 1000 and our spatial lattice to have 10 625 sites. A defect's width was always resolved with more than 12 lattice points. All quantities of interest were computed at given time intervals by averaging over the ensemble.

To perform the numerical evolution, we used a second order staggered leapfrog method. The corresponding set of equations for the field and its conjugate momentum are

$$\begin{aligned} \Pi(x, t + 1/2 \delta t) &= \frac{1 - \chi}{1 + \chi} \Pi(x, t - 1/2 \delta t) \\ &+ \frac{\delta t}{1 + \chi} [\nabla^2 \phi(x, t) + \phi(x, t) - \phi^3(x, t)], \end{aligned} \quad (2.23)$$

$$\phi(x, t + \delta t) = \phi(x, t) + \delta t \Pi(x, t + 1/2 \delta t), \quad (2.24)$$

where  $\chi = \tilde{\eta} \delta t / 2$  and  $\delta t$  is the time step.

The initial conditions were generated in Fourier space using a normal distributed random number generator and then converted to real space using a fast Fourier transform algorithm. For each chosen time step we measured the average density of zeros of the field (by looking at sign changes at consecutive lattice points), the average density of defects (by counting the number of zeros in the coarse-grained field), and the correlation function. Using the correlation function, we have calculated the correlation length which we defined as the point at which the value of the correlation function, normalized at zero spacing to be unity, goes below  $1/e$ . This also enables us to define defect and zero densities per correlation length volume.

Several precautions should be taken in order to guarantee a good accuracy of the results. The spatial step should be small enough to resolve the defects and the time step should obey the Courant condition

$$\delta t \ll \delta x,$$

where  $\delta x$  is the physical lattice spacing, in order for the method to converge safely.

## III. THE RESULTS

### A. Testing our methods and exact analytical results for the Gaussian theory

The simplest test we can perform on our procedure is to measure the zero densities in our numerical evolution in the special case of  $\lambda = 0$  and compare the results to the exact predictions of the linearized theory.

This involves several aspects of our numerical data. Firstly, we want to test whether our randomly generated initial conditions reproduce faithfully an average field configuration out of Boltzmann distribution and, in the affirmative case, whether the numerical evolution in the simple case of the linear theory coincides with the exact analytical results derived in Secs. II C and II D.

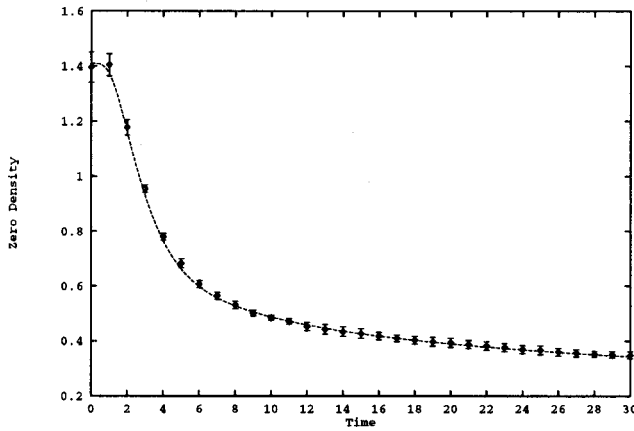


FIG. 1. Exact Linear evolution (solid line) and numerical evolution (data points) for the zero density in the free case. The error bars denote the standard deviation from the mean, computed over our ensemble of 128 realizations.

In order to do the latter, we must necessarily introduce an ultraviolet momentum cutoff  $\Lambda$ . We note, however, that Halperin's formula is still applicable for a finite number of modes, the exact result being given by Eq. (2.22) with finite limits in the sum. Therefore the unavoidable introduction of a cutoff should not be an obstacle to the numerical verification of the analytical predictions. Before comparing the zero density obtained from the numerical linear evolution to the exact result, we must pay attention to one last technical complication. When converting a finite set of amplitudes generated in  $k$  space to  $x$  space using the fast Fourier transform algorithm, we are actually losing resolution, in the sense of field structure, in the smallest scales, which in turn can lead to an underestimate of the number of zeros. We observed explicitly this problem when transforming a generated field configuration with  $N$  amplitudes in momentum space to a grid with the same number of points in configuration space. A simple way of overcoming this difficulty is to, for a chosen  $\Lambda$ , generate an extra number of modes of higher momentum with zero amplitude and then transform this set to  $x$  space. This corresponds basically to an increase in the number of points in real space (and, thus, in the spatial resolution), while keeping a given momentum cutoff fixed. How much precision we actually need then is decided by increasing the number of extra modes with zero amplitude until the average zero density converges to the analytical result for the Boltzmann distribution, given by Eq. (2.23). We were careful to follow this procedure even when the comparison to the linear results was unnecessary, in the case of the full classical evolution.

Having done this, we obtained an excellent agreement between the initial conditions and their numerical evolution and the exact analytical result, with a very small standard deviation within our ensemble, represented by the error bars in Fig. 1.

This also reassured us that the number of samples used in our ensemble, 128 as mentioned above, is large enough for us to obtain a good approximation to the exact ensemble averaged quantities.

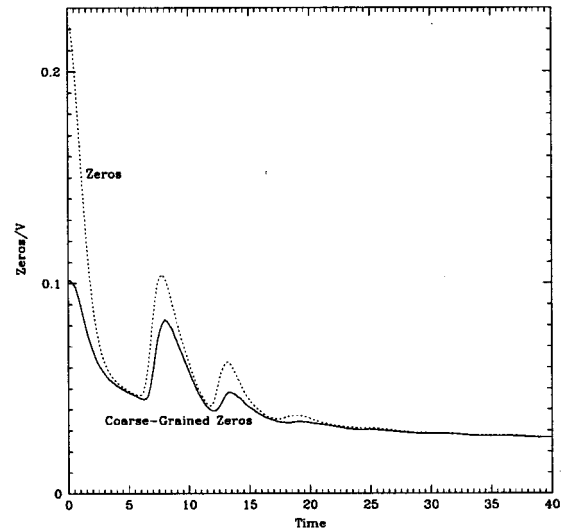


FIG. 2. Evolution of the total zero density and that in the coarse-grained field on the scale of the width of a defect for  $\eta=0.05$  and initial conditions with  $M=0.1$ ,  $T=0.005$ . For late times the coarse-grained zeros can be identified as topological defects.

## B. Nonlinear field and defect evolution

Having performed the tests of Sec. III A, we are now ready to analyze the evolution of the field in the presence of the nonlinear term. As mentioned before, the evolution results depend only on one dynamical parameter  $\tilde{\eta}$  and on the initial conditions which are specified completely by the values of the temperature,  $1/\beta$ , and the mass  $M$ . In what follows we will assume the rescaled evolution of Eq. (2.3) and drop tildes.

An example of the zero and defect density evolution is shown in Fig. 2. As expected the density of the latter is always smaller than that of the former and independent of the chosen momentum cutoff. We also observe that for reasonably dissipated systems, the defect and zero densities coincide for large times. The zero densities observed in the coarse-grained Gaussian initial field should not be taken strictly as defects, off course, as they lack the stability only obtained at later times when the field truly settles down locally at either of the energetically equivalent minima.

The qualitative evolution of the field, in the aftermath of a sudden quench, can be seen to follow two quite different stages. Firstly, immediately after the quench, the negative curvature of the potential near the origin gives rise to instabilities in the fields, in the sense that if one neglects the cubic term in the evolution, which is initially taken to be small [because  $\langle \phi^2(t=0) \rangle \ll 1$ , by construction] the modes with momentum  $k < k_c$  will evolve according to the exponential forms of Eq. (2.17). The corresponding exponential growth distorts the original field configuration since the amplitudes for the unstable modes grow much larger than their characteristic value, typical of the thermal initial conditions, while the remaining amplitudes stay approximately the same, but for damping if dissipation is present. The result of this evolution is a considerable deviation from the Boltzmann distributed initial field. This characteristic unstable behavior suggests that it is a good working hypothesis to assume that the field in this initial stage follows approximately the lin-

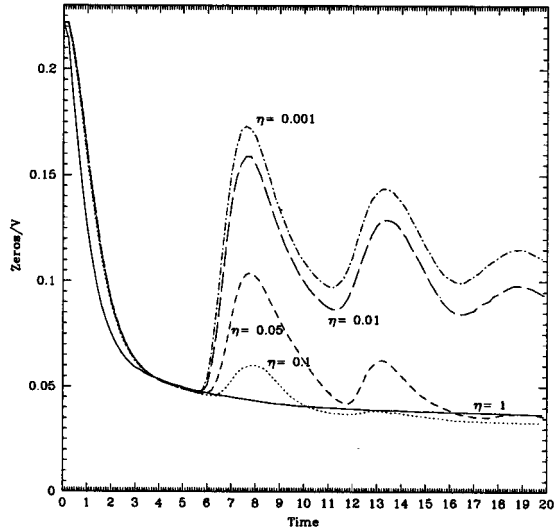


FIG. 3. Evolution of the zero density for different values of  $\eta$  and initial conditions with  $M=0.1$  and  $T=0.005$ .

earized evolution. We will check and confirm this conjecture in what follows.

The instabilities shut down when the cubic term, in Eq. (2.3), grows large enough to compensate for the negative sign of the mass. This is the beginning of the second stage of the evolution, often referred to in the literature as reheating since the field during this period tends again to a new maximum entropy configuration. The evolution at this stage is completely nonlinear and inaccessible through the usage of a weak-coupling perturbative expansion.

At the beginning of reheating, the fields are severely red shifted relative to a thermal distribution and energy redistribution among the modes must occur. As a result, in the absence of strong dissipation, the amplitude of the short wavelength modes grows while that of the long wavelength modes decreases. These two types of behavior are now not just characteristic of modes with momentum  $k > k_c$  and  $k < k_c$ , respectively, since among the latter the amplitude also has grown differentially, approximately with the exponential of their characteristic frequency, Eq. (2.17). As a result of this flow of energy to smaller wavelengths, the field configurations change to display much more structure on smaller scales including those in which topological defects can be produced. After the first burst of energy transfer to smaller scales, the resulting field configurations involving large gradients are disfavored energetically and the field evolves back quickly to suppress them partially. This results in a series of oscillations in typical quantities, such as the zero densities or the correlation length, Fig. 3 and Fig. 8.

In the presence of external dissipation, for  $\eta$  nonzero, the instabilities grow in an analogous way, soon after the quench, but the process of energy redistribution or reheating can be quite different. The presence of external dissipation, as we discussed above, can be seen as resulting from the existence of effective channels, i.e., modes of other fields, which compete with those of the scalar field for the energy transferred from its largest wavelength modes. The value of  $\eta$  then determines the relative importance of these two types of channels. This competition among scalar field and chan-

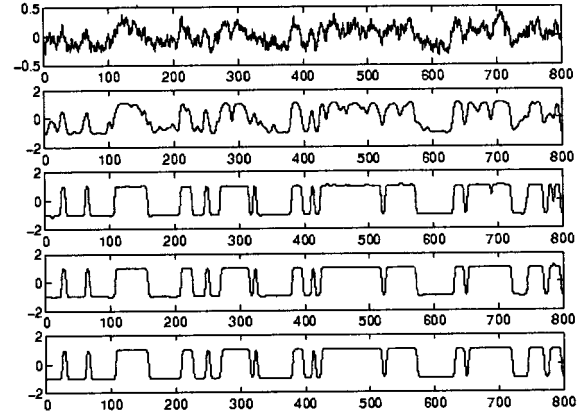


FIG. 4. Field profiles at different instants of the evolution for  $\eta=1$  and initial conditions with  $M=0.1$  and  $T=0.005$ . It is evident that the field configuration is frozen in for the larger times.

nels external to it turns out to be absolutely crucial for the form of the evolution of the zero and defect densities.

Schematically, with our choice of parameters, for  $\eta=1$ , the system is always strongly dissipated and behaves much like a field without self-interactions (albeit stable) that freezes in very early. This can be seen clearly in the field profiles of Fig. 4. The effective external channels, therefore, dominate strongly over the scalar field self-interactions and no signature of reheating, such as the creation of zeros or a strong drop in correlation length, is observable.

For smaller values of the dissipation,  $\eta=0.1-0.05$ , both self-interactions and dissipation are important, acting on the same kind of time scales. It is clear from our results that the transfer of amplitude among the modes occurs at well-defined stages of their oscillations. This is a subject of study in its own right, which is beginning to receive much attention in the context of the theory of reheating after a period of inflationary expansion in the early Universe. Our objective in this paper is not to tackle this question, but, in view of the strong analogies between the two problems, to point out merely that as a consequence of this behavior the creation of zeros and defects at reheating proceeds by bursts. This is visible in Fig. 5.

When zeros and defects are created in these bursts, the dissipation (if not high enough) and the field self-interactions are not sufficiently effective to suppress them immediately. As the momentary production shuts off, however, both these processes reduce the zero densities considerably. At the next burst another large amount of small scale structure can be created again, but smaller than that at the previous instance. The field evolution then proceeds to dissipate it away and so on. As a result of these two competing processes, the field oscillates between having quite large amounts of structure on small scales and having little, as both processes of creation and dissipation seem to be most efficient after the converse one has acted. These processes are clearly visible in the large oscillations undergone by the correlation length and defect densities. Profiles out of a field evolution in this dissipative regime is shown in Fig. 6.

Finally, for small values of the dissipation coefficient,  $\eta \leq 0.01$ , the field is allowed to reach a favorable configura-

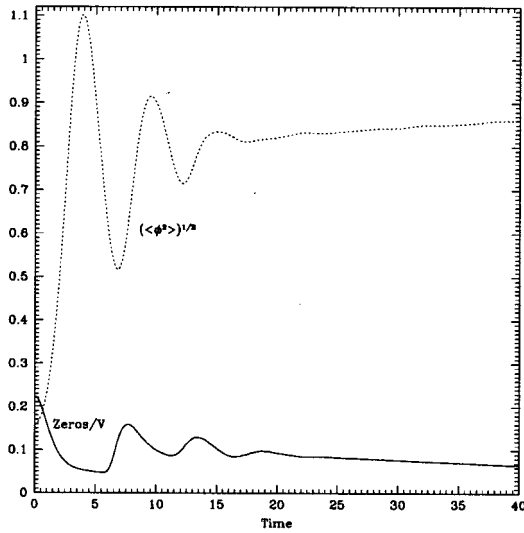


FIG. 5. The production of zeros at reheating and the mean-field squared evolution. It is clear that zero production proceeds by bursts.

tion before the dissipation has any sizable effect. The zero densities still oscillate in a similar fashion, but field ordering in small scales now seems to be due to essentially the action of the field self-interactions. For this same reason the densities for large times are much larger than those obtained under the presence of larger dissipation. Its effect, if present at all, is only to damp all modes for large times. Modes on smaller scales are more strongly dissipated, though, due to the fact of possessing a larger natural frequency. Snapshots of the field out of a characteristic evolution under the effect of very weak dissipation can be seen in the field profiles of Fig. 7.

Equivalently, the field evolution can be studied qualitatively by considering the time dependence of the correlation length. Figure 8 shows the behavior of the correlation length in time under the effect of several values of the external dissipation.

It is clear that the correlation length increases in the first quasilinear stage of the evolution, decreases at reheating and increases again as the field organizes itself both via the effect

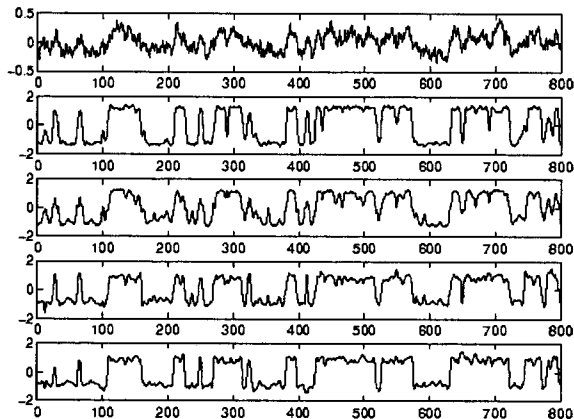


FIG. 6. Field profiles at different instants of the evolution for  $\eta=0.1$  and initial conditions with  $M=0.1$  and  $T=0.005$ .

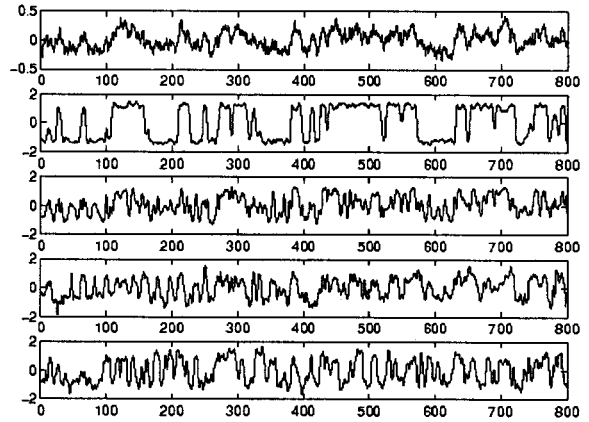


FIG. 7. Field profiles at different instants of the evolution for  $\eta=0.001$  and initial conditions with  $M=0.1$  and  $T=0.005$ . The effects of reheating are clear from the comparison of the second frame to the third.

of its self-interactions and due to the action of the external dissipation.

It is interesting to note, however, that the time evolution of the correlation length for large times, after reheating, seems to display quantitatively different time trends depending on whether the self-organization proceeds by essentially the action of the scalar field self-interactions or results from the effect of the external dissipation. This seems to result in a linear time dependence in the first case and a well-known diffusive behavior with  $t^{1/2}$  in the latter. This is illustrated in Fig. 9, where it is also interesting to note that the slope of the linear correlation length growth for small dissipation is about 0.1 of the speed of light.

This seems to suggest that the underlying field ordering proceeds by the free propagation of a well-defined signal at a fraction of the speed of light as is often suggested in qualitative scenarios for domain formation and growth.

It is, of course, also possible that the linear behavior observed above will constitute merely a transient regime and

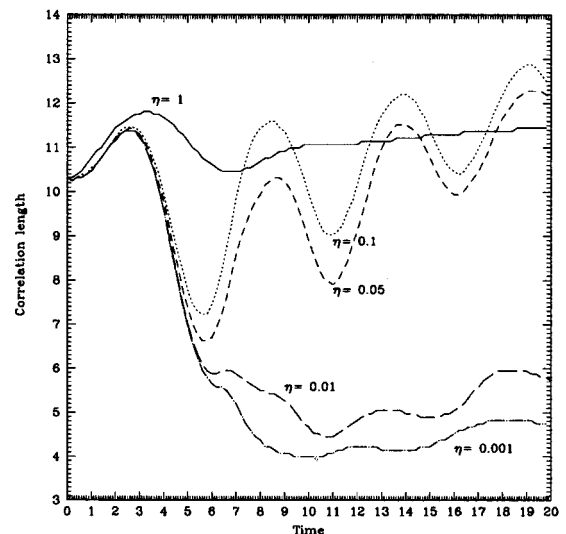


FIG. 8. Time evolution of the correlation length for  $M=0.1$ ,  $T=0.005$ , and several values of the dissipation  $\eta$ .



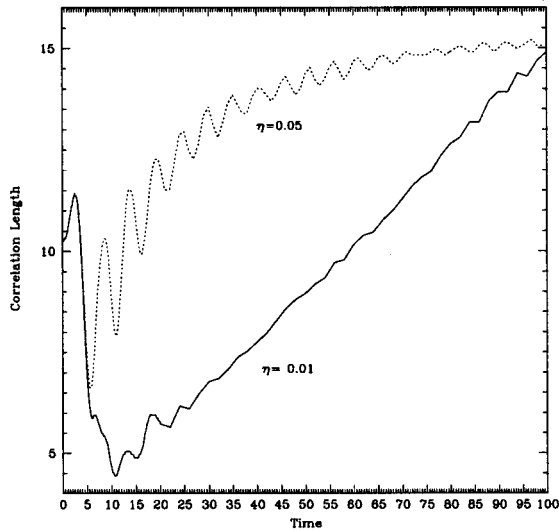


FIG. 9. Long time evolution of the correlation length for initial conditions with  $M=0.1$ ,  $T=0.005$ ,  $\eta=0.01$ , and  $\eta=0.05$ . For the smaller of these values, the correlation length evolves linearly with coefficient 0.1 whereas for the larger dissipation, it displays approximately diffusive behavior.

that the evolution of the correlation length actually follows the same diffusive pattern, obtained under the effect of larger dissipation, but on a much larger time scale. For even smaller values of  $\eta$  we observed the persistence of the linear behavior, but with smaller slopes, showing that the external dissipation is still playing a role in the field's self-organization.

We also tried to determine the influence of our choice of initial conditions on the evolved defect densities. Initially, for an average Boltzmann field in the continuum limit, the spatial two-point correlation function has the exact form

$$\langle \phi(x) \phi(x') \rangle = \pi \frac{T^3}{M} e^{-M|x-x'|}. \quad (3.1)$$

This defines unambiguously the correlation length to be  $\xi=1/M$ . Different choices of initial conditions corresponding to different masses  $M$ , therefore, lead to quite distinct field configurations on given scales. Figure 10 shows the defect density evolution for a choice of low dissipation,  $\eta=0.01$ , and three different initial masses.

The initial temperature was chosen so as to guarantee that the field undergoes initial instabilities, i.e., so as to ensure the effectiveness of the quench as the mechanism driving the transition. The values chosen were such that  $\langle \phi(t=0)^2 \rangle \sim 0.1$ , in our original Boltzmann distributed field. This results in small values of the temperature relative to the mass scales, of the order  $M/T \sim 0.01-0.05$ . It should be noted, however, that the initial zero and defect densities are independent of this choice of temperature.

Given a choice of  $M$  and the associated correlation length  $\xi=1/M$ , we expect, in rough terms, that the defect densities will be larger for smaller  $\xi$ , as this is a qualitative indication of more structure on smaller scales. This can be seen clearly by comparing the initial magnitudes of the defect densities in Fig. 10, for three different choices of initial correlation lengths.

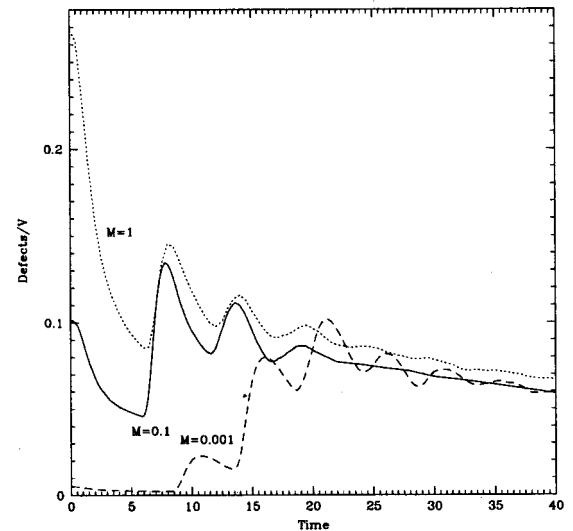


FIG. 10. Defect density evolution for three different initial conditions, with  $M=1$ ,  $T=0.02$ ,  $M=0.1$ ,  $T=0.005$ , and  $M=0.001$ ,  $T=1.10^{-5}$ .

Figure 10 shows a much more striking fact, however. It is clear that the number of defects produced at the phase transition is approximately independent of the initial densities even when these differ by over an order of magnitude. This is a clear indication of the importance of accounting correctly for the number of defects present at the time of reheating and not sooner. This observed independence of the choice of initial defect densities is only characteristic of evolutions under the effect of small or null dissipation as in strongly dissipated systems reheating is, as we have seen above, severely suppressed.

### C. Comparison with the results from the linearized theory and the Hartree approximation

In the previous section we presented and discussed the results for the full classical evolution of Eq. (2.3). In view of their extensive application to nonequilibrium problems in the literature, it is extremely interesting to analyze how particular approximations to this classical theory perform relative to it.

In this subsection we compare briefly the results for the zero density evolution given by the full classical evolution to those obtained in the Hartree evolution and by considering the free field given by the linearized theory.

Figure 11 and Fig. 12 show two examples of the zero-density evolution computed in these three cases, and for relatively low and high dissipation, respectively. The observed difference between the zero densities given by the full classical evolution and those of the linear theory is quite simple to understand. For large  $\eta$ , as we discussed above, the effective channels present implicitly in the form of the dissipation kernel, predominate over the scalar field self-interactions. As a result, under large dissipation, the observed evolution for the zero density is quite similar to that of a linear field, following approximately the results obtained by replacing, Eq. (2.17) into the expression for the zero density of a Gaussian theory, Eq. (2.18). This procedure yields

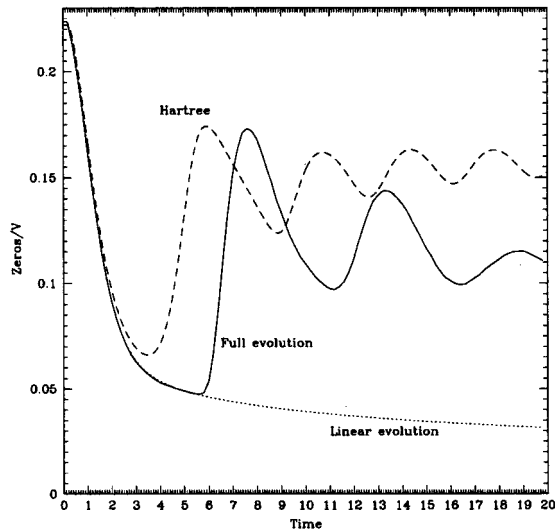


FIG. 11. The zero density given by the full classical, linearized, and Hartree evolutions for  $\eta=0.001$  and initial conditions with  $M=0.1$  and  $T=0.005$ .

$$\langle n(t) \rangle \sim 1/(k_c t)^{1/2}. \quad (3.2)$$

Perhaps the most interesting feature of Eq. (3.2) is that it constitutes a lower bound on the defect density obtained from the classical theory, computed with the same initial field configuration at the same instant in time, for an evolution with any given  $\eta$ . This fact remains interesting only for times that are not too large, since the field evolution under high dissipation freezes quickly in with a definite number of defects (see Fig. 5), while Eq. (3.2) tends hopelessly to zero densities as time increases. This discrepancy for large times can be seen clearly in Fig. 13.

In contrast to the previous situation, for evolutions under small external dissipation, the discrepancies between the zero density computed from the full classical theory and the

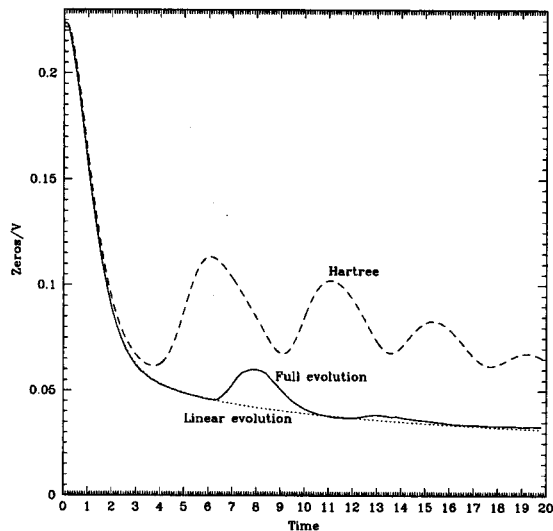


FIG. 12. The density of zeros given by the full classical, linearized, and Hartree evolutions for  $\eta=0.1$  and initial conditions with  $M=0.1$  and  $T=0.005$ .

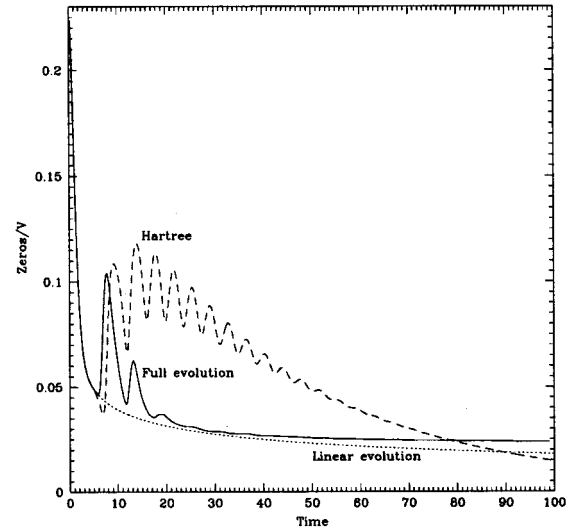


FIG. 13. The density of zeros given by the full classical, linearized, and Hartree evolutions for  $\eta=0.05$  and initial conditions with  $M=0.1$  and  $T=0.005$ .

linearized theory are quite dramatic at the time of reheating. The reheating process is accompanied by the production of a large number of zeros and defects that naturally go completely unaccounted for by the linear evolution. This is clearly visible in Fig. 11.

The results obtained using the Hartree evolution also fail to reproduce those of the full classical evolution, but in somewhat the opposite way. At reheating the flow of energy from the infrared to all other modes is very efficient in the Hartree evolution. When  $\eta$  is small this indeed results in essentially the same number of created zeros as in the full evolution, as can be seen, e.g., in Fig. 11. The collisionless character of the approximation, however, precludes the field from ridding itself of high gradient configurations. This results in the fundamental difference between the Hartree and the full evolution that, in the absence of dissipation, the number of zeros decreases in the latter, but remains approximately constant after creation in the former. For short times, of the order of up to  $t=20-30$ , the Hartree approximations, therefore, yield a number of zeros always larger than the full classical evolution. For larger times and for reasonably dissipated systems ( $\eta \geq 0.05$ ), the fact that the Hartree approximation leads to field configurations with more structure on small scales than the full evolution, implies that it can be dissipated more efficiently. The end result is that after the dissipation makes its effect noticeable, the zero density resulting from the Hartree evolution is smaller than that of the full theory. For sufficiently large times, such densities, nevertheless, tend to a constant value thus freezing in, as in the case of the full classical theory, unlike what happens in the case of the linear evolution.

For evolutions under stronger dissipation and for relatively short times, such as can be seen in Fig. 12, the discrepancy between the Hartree and the full classical evolution can be quite spectacular and the linear result turns out to constitute a much better approximation. This is a clear concrete example in which the presence of a truncated set of

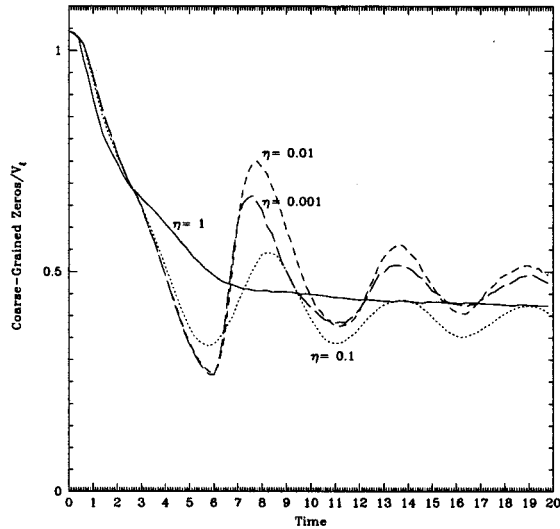


FIG. 14. The evolution of the defects densities per correlation volume for several values of  $\eta$ , for initial conditions with  $M=0.1$  and  $T=0.005$ .

interactions actually leads to a much worse prediction than what could be obtained much more simply from a trivial, exactly solvable linear approximation.

#### D. Correlation volume defect densities, scaling, and the Kibble mechanism

The evolution of the defect densities and of the field's correlation length are interesting in their own right. However, it is clear that they can constitute two different ways of probing the same qualitative structure. Defects are associated with sites of space where the field changes quickly between its two distinct energetically equivalent minima and constitute, therefore, regions where the field two-point correlation decreases. For this very reason defect densities tell us statistically how many areas of almost fully correlated field exist in a given volume, allowing us to probe their mean characteristic size. This is, in turn, clearly a measure of the correlation length.

The defect densities per correlation length volume  $V_\xi$  constitute, therefore, very interesting quantities, that lie at the basis of fundamental conjectures for defect and domain formation and evolution such as the Kibble mechanism and scaling conjectures.

In Figs. 14 and 15 we plot these densities for two different sets of initial conditions, with large and small initial correlation length, respectively.

The Kibble mechanism invokes precisely the value of the field's correlation length in order to predict the defect density produced at a symmetry breaking phase transition. The correlation length is clearly a qualitative measure of the size of the volume over which the field has only small amplitude fluctuations. Defects on the other hand correspond to field configurations that interpolate between the energetically indistinguishable minima and, therefore, should lie at the boundaries of average correlated patches. At distances larger than the correlation length, the field will be in either one of these minima. The Kibble mechanism further assumes in what is usually designated the geodesic rule that between

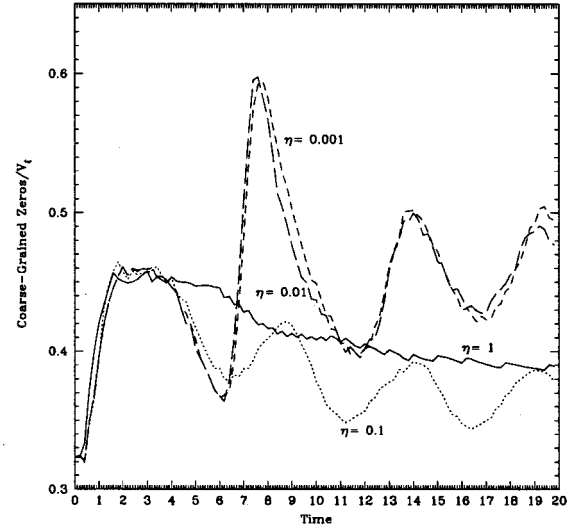


FIG. 15. The evolution of the defects densities per correlation volume for several values of  $\eta$ , for initial conditions with  $M=1$  and  $T=0.02$ .

such uncorrelated regions, the continuous field should take the shortest path over its vacuum manifold. This results in the simple, but powerful prediction that between two correlation volumes, in one spatial dimension, there will be a defect or not with probability of 1/2. This is, naturally, the predicted value for the correlation volume defect density.

Observing Figs. 14 and 15, it is quite striking to notice that regardless of the value of  $\eta$  and of the particular choice of initial conditions, the defect densities obtained at reheating and, thereafter, are of the order of the prediction given by the Kibble mechanism within a factor of about 10%.

During the stage of reheating, it is still quite apparent that energy transfers between different scales are large and that arguments based on local-energy minimization will be much blurred by large fluctuations [20]. Consequently, it is more interesting to investigate the behavior of the defect densities for times sufficiently large that the system will have found already an energy balance among all scales. Figure 16 shows the evolution of the defects densities per correlation volume, for two relatively close low values of dissipation,  $\eta=0.05$  and  $\eta=0.01$ , and a larger time range. It is clear that the correlation volume density of defects tends to a constant for large times. This is evidence for the scaling behavior of the domain wall network, i.e., for the fact that the number of defects per correlation volume remains constant in time, approximately once reheating is complete.

This is an extremely powerful observation as it states that the *statistical* evolution of a domain wall network is characterized by one single length scale. According to this conjecture, the domain wall network is self-similar after rescaling, when in the scaling regime, and its statistical features can be known at all times given the knowledge of the correlation length. Figure 16 also shows clearly that, for the same value of dissipation, but different initial conditions, the correlation length defect densities for evolutions under small dissipation result in the same large time defect densities. This is evidence for the fact that the scaling densities are in these circumstances also independent of the initial conditions, chosen at energies above the transition.

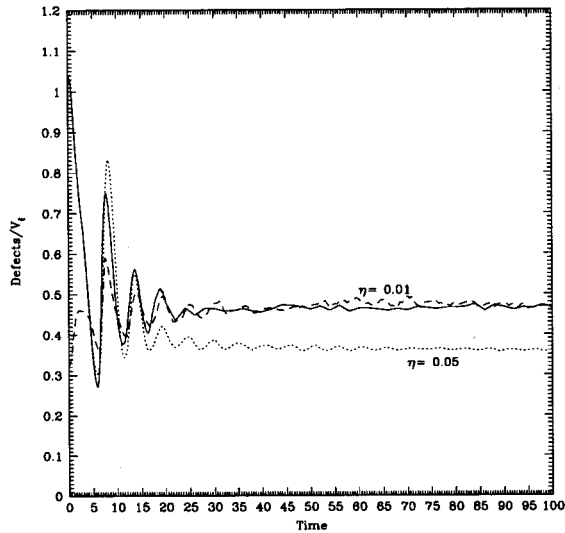


FIG. 16. The evolution of the defects densities per correlation volume for two values of  $\eta$ . For  $\eta=0.01$  the dashed line corresponds to initial conditions with  $M=1$  and the solid line with  $M=0.1$ . The scaling regime for large times is apparent as well as the corresponding defect density independence on the choice of initial conditions for  $\eta=0.01$ .

Moreover, the value for the defect density in the scaling regime, accepting the criterion of Sec. II E for determining the correlation length, for the smaller dissipation parameter in Fig. 16, is very close to that predicted by the Kibble mechanism. In contrast, it is extremely interesting to notice that for a slightly larger value of  $\eta$ , the scaling defect density is about 10% lower. This seems to indicate that the presence of additional degrees of freedom that compete with those of the scalar field for its energy, necessarily leads to scalar field configurations with lower scaling defect densities.

For evolutions under stronger dissipation, the scaling regime is of no particular interest, however, as it corresponds to the trivial situation in which the field is frozen in and both defect densities and correlation length become constant in time. Both these remarks may have interesting realizations as scenarios for defect formation in the early Universe.

#### IV. CONCLUSIONS

We presented a detailed study of the nonequilibrium dynamics of a classical scalar field theory in a symmetry breaking transition. In doing so we were able to probe regimes of field evolution where perturbation theory breaks down and extract conclusions about the detailed correlation length and topological defect density evolution. We showed that after an instantaneous quench a field develops momentary instabilities responsible for the growth of its amplitude during which the evolution is approximately linear, and on a later stage when stability around the true minimum is found evolves, in a period of reheating very similar to that of inflationary scenarios. During this later stage the evolution proceeds in a strongly nonlinear fashion so as to redistribute energy among all scales. We showed the effect of external dissipation in the

evolution and established evidence for the independence of defect densities per correlation length on the choice of initial conditions as well as their approach to a scaling regime for large times. In passing we confronted the predictions of the Kibble mechanism to our results and discussed the effect of the external dissipation on the asymptotic defect densities. We also have shown the comparison between the zero densities given by the full classical evolution and the predictions from the linearized theory and the Hartree approximations thus clarifying when these approximate schemes are valid.

Finally, we believe that the present work raises many new important questions about the evolution of relativistic fields away from thermal equilibrium. We have established the utmost importance for the correct accounting of the transfers of energy from the Higgs field to other channels and their influence in defect formation. In higher spatial dimensions, we believe these transfers will be magnified by the increase in phase space and, consequently, in the number of external channels coupled to the long wavelength modes of the scalar field. These energy transfers are responsible for the assumptions of freeze-out of the defect densities both in the Kibble mechanism [1] and in the Zurek scenario [8], which constitute the basis for defect formation estimates in the early Universe and in the laboratory. In the former the correct accounting of the expanding background as the mechanism driving the transition is fundamental in relating the microphysical dynamical scales to the horizon. In adopting the instantaneous quench in the work described in this paper, we merely have taken the simplest workable example of symmetry breaking.

We are investigating presently the effect of an expanding background on topological defect production and evolution, in higher spatial dimensions, and studying the details of the energy redistribution during the phase transition. The major difficulties of these studies have to do with the enormous disparity between the microphysical and cosmological scales and the need for renormalization in spatial dimensions higher than one.

Whenever we can overcome these difficulties, field theoretical studies of cosmological phase transitions will clarify important aspects of the role of topological defects as the seeding mechanism for the formation of structure in the Universe and the theory of reheating after a period of inflationary expansion.

#### ACKNOWLEDGMENTS

It is a great pleasure for us to thank Salman Habib, Wojciech Zurek, and Marcelo Gleiser for extremely useful suggestions. We also thank Ed Copeland, Ray Rivers, and Graham Vincent for discussions and Alisdair Gill for comments on the manuscript. The research of N.D.A. and L.M.A.B. was supported by J.N.I.C.T.- *Programa Praxis XXI*, under Contracts No. BD/2794/93-RM and No. BD/2243/92-RM, respectively. This work was supported in part by the European Commission under the Human Capital and Mobility program, Contract No. CHRX-CT94-0423. We thank The Fujitsu/Imperial College Centre for Parallel Computing for generous allocation of resources.

- [1] T. W. B. Kibble, *J. Phys. A* **9**, 1387 (1976).
- [2] For a comprehensive review, see A. Vilenkin and E. P. S. Shellard, *Cosmic Strings and other Topological Defects* (Cambridge University Press, Cambridge, England, 1994).
- [3] P. C. Hendy, N. S. Lawson, R. A. M. Lee, P. V. E. McLintock, and C. D. H. Williams, *Nature (London)* **368**, 315 (1994).
- [4] V. M. H. Ruutu *et al.*, *Nature (London)* (to be published).
- [5] I. Chuang, R. Durrer, N. Turok, and B. Yurke, *Science* **251**, 1336 (1991); M. J. Bowick, L. Chander, E. A. Schiff, and A. M. Srivastava, *ibid.* **263**, 943 (1994).
- [6] T. Vachaspati and A. Vilenkin, *Phys. Rev. D* **30**, 2036 (1984).
- [7] Ya. B. Zeldovich, *Mon. Not. R. Astron. Soc.* **192**, 663 (1980); A. Vilenkin, *Phys. Rev. Lett.* **46**, 1169 (1981); **46**, 1496(E) (1981).
- [8] W. H. Zurek, *Phys. Rep.* (to be published); *Acta Phys. Pol. B* **24**, 1301 (1993).
- [9] D. Boyanovsky, D.-S. Lee, and A. Singh, *Phys. Rev. D* **48**, 800 (1993).
- [10] D. Boyanovsky and H. J. de Vega, *Phys. Rev. D* **47**, 2343 (1993); H. J. de Vega and R. Holman, *ibid.* **49**, 2769 (1994); D. Boyanovsky, H. J. de Vega, D.-S. Lee, and A. Singh, *ibid.* **51**, 4419 (1995).
- [11] F. Cooper, S. Habib, Y. Kluger, E. Mottola, J. P. Paz, and P. R. Anderson, *Phys. Rev. D* **50**, 2848 (1994).
- [12] A. J. Gill and R. J. Rivers, *Phys. Rev. D* **51**, 6949 (1995); G. Karra and R. J. Rivers, Imperial College Report No. Imperial/TP/95-96/28 and hep-ph/9603413 (unpublished).
- [13] G. Parisi, *Statistical Field Theory* (Addison-Wesley, Reading, MA, 1988).
- [14] N. D. Mermin and H. Wagner, *Phys. Rev. Lett.* **22**, 1133 (1966).
- [15] N. D. Antunes and L. M. A. Bettencourt (in preparation).
- [16] S. Habib and H. E. Kandrup, *Phys. Rev. D* **46**, 5303 (1992).
- [17] B. I. Halperin, in *Physics of Defect*, Proceedings of Les Houches, Session XXXV, 1980, NATO ASI, edited by R. Balian, M. Kléman, and J.-P. Poirier (North-Holland, Amsterdam, 1981), p. 816. For a more comprehensive derivation, see F. Liu and G. F. Mazenko, *Phys. Rev. D* **46**, 5963 (1992).
- [18] F. J. Alexander, S. Habib, and A. Kovner, *Phys. Rev. E* **48**, 4284 (1993).
- [19] S. J. Chang, *Phys. Rev. D* **12**, 1071 (1975).
- [20] L. M. A. Bettencourt, T. S. Evans, and R. J. Rivers, *Phys. Rev. D* **53**, 668 (1996).